Physics of Plasmas

Universality of Poisson-driven plasma fluctuations in the Alcator C-Mod scrape-off layer

Cite as: Phys. Plasmas **25**, 122309 (2018); https://doi.org/10.1063/1.5064744
Submitted: 08 October 2018 . Accepted: 30 November 2018 . Published Online: 18 December 2018

A. Theodorsen, O. E. Garcia, R. Kube, B. LaBombard, and J. L. Terry

View Online Export Citation CrossMark

ARTICLES YOU MAY BE INTERESTED IN

Wavelet methods for studying the onset of strong plasma turbulence
Physics of Plasmas **25**, 122310 (2018); https://doi.org/10.1063/1.5062853

Intermittent fluctuations in the Alcator C-Mod scrape-off layer for ohmic and high confinement mode plasmas
Physics of Plasmas **25**, 056103 (2018); https://doi.org/10.1063/1.5018709

Blob velocity scaling in diverted tokamaks: A comparison between theory and simulation
Physics of Plasmas **26**, 032302 (2019); https://doi.org/10.1063/1.5080675

© 2018 Author(s).

PHYSICS OF PLASMAS **25**, 122309 (2018)

Universality of Poisson-driven plasma fluctuations in the Alcator C-Mod scrape-off layer

A. Theodorsen,[1,a)] O. E. Garcia,[1,b)] R. Kube,[1] B. LaBombard,[2] and J. L. Terry[2]
[1]*Department of Physics and Technology, UiT The Arctic University of Norway, N-9037 Tromsø, Norway*
[2]*MIT Plasma Science and Fusion Center, Cambridge, Massachusetts 02139, USA*

(Received 8 October 2018; accepted 30 November 2018; published online 18 December 2018)

Large-amplitude, intermittent fluctuations are ubiquitous in the boundary region of magnetically confined plasmas and lead to detrimental plasma-wall interactions in next-generation, high duty cycle fusion power experiments. Using gas puff imaging data time series from the scrape-off layer in the Alcator C-Mod device, it is here demonstrated that the large-amplitude fluctuations can be described as a super-position of pulses with a fixed shape and a constant duration. By applying a new deconvolution algorithm on the data time series with a two-sided exponential pulse function, the arrival times and amplitudes of the pulses can be estimated, and the measurement time series can be reconstructed with high accuracy. The pulse amplitudes are shown to follow an exponential distribution. The waiting times between pulses are uncorrelated, their distribution has an exponential tail, and the number of arrivals is a linear function of time. This demonstrates that pulse arrivals follow a homogeneous Poisson process. Identical statistical properties apply to both ohmic and high confinement mode plasmas, clearly demonstrating the universality of the fluctuation statistics in the boundary region of Alcator C-Mod. *Published by AIP Publishing.*
https://doi.org/10.1063/1.5064744

I. INTRODUCTION

Extensive scientific investigations have revealed that cross-field transport of particles and heat in the scrape-off layer (SOL) of magnetically confined plasmas is caused by radial motion of blob-like filament structures.[1–5] This poses several challenges for future magnetic fusion energy reactors, including enhanced erosion rates of the main chamber walls.[6–10] There is also strong evidence that the turbulence-driven cross-field transport is related to the empirical discharge density limit.[11–15] The fluctuation-induced transport and associated plasma–wall interactions evidently depend on the amplitude of the filaments and their frequency of occurrence.[16–18]

Radial and toroidal/poloidal motion of blob-like structures results in single-point recordings dominated by large-amplitude bursts. Recently, a stochastic model was introduced, describing the fluctuations as a super-position of uncorrelated pulses with an exponential shape and a constant duration.[16–20] Predictions of this model, including the probability density function and the frequency power spectral density, are in excellent agreement with Langmuir probe and gas puff imaging (GPI) measurements obtained in ohmic and low confinement modes (L-modes) of several tokamak devices.[21–28]

In this paper, a new method is introduced in order to reveal the pulse amplitudes and arrival times directly, without inferring their properties from the predictions of the model. This is achieved by reformulating the stochastic model as a convolution of the pulse function with a train of delta pulses and invoking a deconvolution algorithm. Applying this method to measurement data from GPI of the SOL in the Alcator C-Mod device, it is for the first time demonstrated that the pulses occur according to a homogeneous Poisson process and that the pulse amplitudes are exponentially distributed. These statistical properties are identical for both ohmic and high confinement modes (H-modes), providing further evidence for universality of the statistical properties of the fluctuations in the boundary region of magnetically confined plasmas. The results presented here complement and extend the previous work that pointed out similarities between SOL plasma fluctuations in L- and H-modes.[26,29–33] In particular, it extends the work reported by Garcia *et al.*[26] by using the new deconvolution method, and the results presented in this contribution should be compared with the results from conditional averaging in the study by Garcia *et al.*[26]

II. EXPERIMENTAL SETUP

Here, deuterium fuelled plasmas in a lower single null divertor configuration were analyzed in all the experiments. The GPI diagnostic on Alcator C-Mod consists of a 9×10 array of toroidal views of a localized gas puff.[34] The spot size of the horizontal lines-of-sight is 3.8 mm in diameter at the gas cloud. The views are brought via optical fibers to high sensitivity avalanche photodiodes, and the signals are digitized at a rate of 2×10^6 frames per second. In this study, the He I line emission from the localized He gas puff is investigated for a view position in the far SOL with a major radius of $R = 90.69$ cm and a vertical position of $Z = -2.99$ cm, which is 1.0 to 1.8 cm outside the last closed magnetic flux surface for the cases studied here.

We will investigate time series from the GPI diagnostic for various plasma parameters and confinement modes as

[a)]Electronic mail: audun.theodorsen@uit.no
[b)]Electronic mail: odd.erik.garcia@uit.no

listed in Table I. All time series have a duration of 100 ms, and these intervals have been chosen such that the time series are approximately stationary without using moving averages or filtering. Two ohmically heated plasma states are analyzed; one low density case is denoted "lO" with a Greenwald density fraction of $\bar{n}_e/n_G = 0.3$, and one high density case is denoted "hO" with a Greenwald fraction of 0.6. Here, $\bar{n}_e$ is the line-averaged electron density and the Greenwald density is given by $n_G = (I_p/\pi a^2)10^{20}\,\mathrm{m}^{-3}$, where the plasma current I_p is given in units of MA, and the minor radius a is in units of meters.[35]

In the case of strong ion cyclotron range of frequency (ICRF) heating, there are two different types of H-modes on Alcator C-Mod without edge localized modes (ELMs). One is the enhanced D-alpha H-mode, here denoted as "eH," which is a steady mode of operation with an edge transport barrier. A quasi-coherent mode in the edge region prevents impurities from accumulating in the core, resulting in a steady state H-mode without ELMs.[36] Another type of ELM-free H-mode on Alcator C-Mod is a quiescent H-mode.[37,38] In this case, there are a strong particle and a heat transport barrier but a lack of macroscopic instabilities in the edge pedestal. This results in a non-steady-state core plasma, with an increasing core density and an accumulation of impurities, which eventually cause a radiative collapse of the plasma. Such a state, here denoted as "qH," has roughly steady-state far SOL plasma parameters and has also been analyzed here. [This "qH-mode" is not the same as and should not be confused with the "QH-mode" found in DIII-D, AUG, JET, and JT-60U, where there are no ELMs, but there is an edge harmonic oscillation (EHO) to provide additional edge particle transport.[39]] A short part of these GPI data time series is presented in Fig. 1, demonstrating the intermittent nature of the fluctuations for all plasma parameters and confinement modes. Here and in the following, the time series are normalized by subtracting the mean value and dividing by the rms-value

$$\widetilde{D} = \frac{D - \langle D \rangle}{D_{\mathrm{rms}}}, \tag{1}$$

where D denotes any of the data time series.

III. FLUCTUATION STATISTICS

In previous work, the predictions of the filtered Poisson process (FPP) have been shown to be in excellent agreement with analysis of experimental measurement data from the SOL of numerous tokamak experiments. The FPP is given by a super-position of uncorrelated pulses[16–20,40–44]

$$\Phi_K(t) = \sum_{k=1}^{K(T)} A_k \varphi\left(\frac{t - t_k}{\tau_d}\right) \tag{2}$$

on the interval $t \in [0, T]$, where T is the full time duration of the signal. All pulses have the same pulse duration time τ_d. The pulse arrival times t_k are independently and uniformly distributed on $[0, T]$. Correspondingly, $K(T)$ is a Poisson process with intensity T/τ_w, and the waiting times are exponentially distributed with mean value τ_w. The amplitudes A_k are taken to be independent and exponentially distributed with the mean value $\langle A \rangle$. The pulse function φ is given by a two-sided exponential function

$$\varphi(x) = \begin{cases} \exp\left(-x/(1-\lambda)\right), & x \geq 0, \\ \exp\left(x/\lambda\right), & x < 0, \end{cases} \tag{3}$$

where x is a unitless variable and λ is the pulse asymmetry parameter restricted to the range $\lambda \in [0, 1]$. The most important parameter describing this process is the *intermittency parameter* $\gamma = \tau_d/\tau_w$, which determines the degree of pulse overlap.[16]

It can be shown that the stationary probability density function (PDF) of the FPP with two-sided exponential pulses is a Gamma distribution with a shape parameter γ and a scale parameter $\langle A \rangle$[17]

$$P_\Phi(\phi) = \frac{\phi^{\gamma-1}}{\langle A \rangle^\gamma \Gamma(\gamma)} \exp\left(-\frac{\phi}{\langle A \rangle}\right), \quad \phi > 0. \tag{4}$$

The four lowest order moments of Φ are given by the mean $\langle \Phi \rangle = \gamma \langle A \rangle$, the variance $\Phi_{\mathrm{rms}}^2 = \gamma \langle A \rangle^2$, the skewness $S_\Phi = 2/\gamma^{1/2}$, and the flatness $F_\Phi = 3 + 6/\gamma$.

In order to account for measurement noise and small discrepancies from the pure two-sided exponential pulse function, we introduce a normally distributed noise signal $X(t)$, with a mean value μ, variance $X_{\mathrm{rms}}^2 = \epsilon \Phi_{\mathrm{rms}}^2$, and the same power spectral density as $\Phi(t)$.[20,42] The *noise parameter* ϵ is defined as

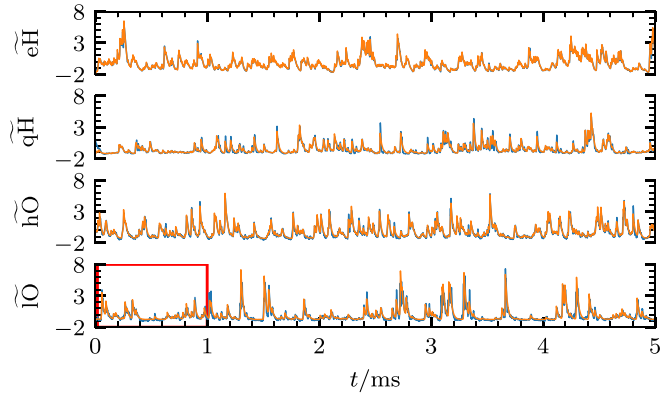

FIG. 1. Excerpt of GPI measurement data time series for four different plasma states (blue lines). Also shown are reconstructed time series from the deconvolution algorithm (orange lines). All time series have been normalized to have zero mean and unit standard deviation. The red box indicates the excerpt presented in Fig. 5.

TABLE I. Notation and shot number for the discharges analyzed here. "lO" denotes the low density Ohmic plasma, "hO" denotes the high density Ohmic state, "qH" denotes the quiescent H-mode, and "eH" denotes the enhanced D-alpha H-mode. Each time series analyzed has a duration of 100 ms, and t_0 gives the starting time. The other columns give the Greenwald fraction of the line-averaged density, the magnetic field on the axis, the plasma current, and the ICRF heating power.

Plasma state	Shot number	t_0/s	n_e/n_G	B_0/T	I_p/MA	P_{RF}/MW
lO	1150618021	0.80	0.3	4.1	0.6	0
hO	1150618036	0.74	0.6	4.1	0.6	0
qH	1110201011	1.13	0.5	5.4	1.2	3.0
eH	1110201016	1.23	0.6	5.4	0.9	3.0

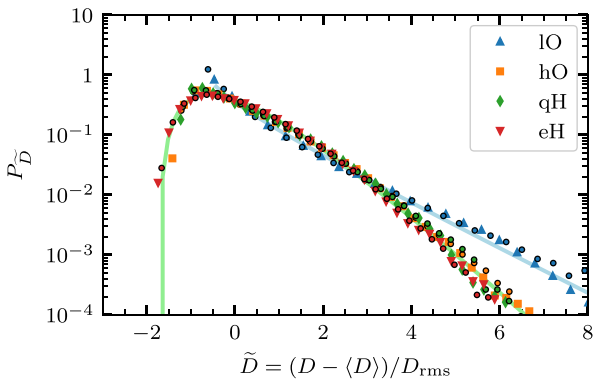

FIG. 2. PDFs of GPI measurement data (symbols), the corresponding distributions from the reconstructed time series (the same color but outlined circles) described in Sec. V, and two Gamma distributions with shape parameters $\gamma = 2/3$ (light blue line) and $\gamma = 3$ (light green line). D denotes any of the original or reconstructed time series.

$$\epsilon = \frac{X_{\rm rms}^2}{\Phi_{\rm rms}^2}. \tag{5}$$

We denote the sum of the FPP with noise as

$$\Psi(t) = \Phi(t) + X(t). \tag{6}$$

The distribution of Ψ is a convolution between a Gamma distribution and a normal distribution, and the first four moments are given by $\langle\Psi\rangle = \mu + \gamma\langle A\rangle$, $\Psi_{\rm rms}^2 = (1+\epsilon)\gamma\langle A\rangle^2$, $S_\Psi = 2[(1+\epsilon)^3\gamma]^{-1/2}$, and $F_\Psi = 3 + 6(1+\epsilon)^{-3}\gamma^{-1}$.[42]

Normalizing Ψ by subtracting the mean and dividing by the rms-value according to Eq. (1) eliminates μ and $\langle A\rangle$ as explicit parameters. In Fig. 2, the PDFs of the measurement data are compared with the Gamma distribution with shape parameters $\gamma = 2/3$ and $\gamma = 3$. By using the method described in Ref. 20, γ and ϵ can be estimated from the empirical characteristic function of the normalized GPI time series. Using these values and the first two moments of the time series, μ can be estimated as $\mu = \langle\Psi\rangle - \sqrt{\gamma/(1+\epsilon)}\Psi_{\rm rms}$ and $\langle A\rangle$ can be estimated as $\langle A\rangle = (\langle\Psi\rangle - \mu)/\gamma$.

The estimated model parameters are presented in Table II along with the mean value of the time series. Consistent with Fig. 1, the low density Ohmic state is strongly intermittent, while pulse overlap is more significant for the enhanced D-alpha H-mode state as expected from the moment estimation. In all cases, ϵ is very moderate, or practically vanishing, consistent with the good agreement between the data and a pure Gamma distribution in Fig. 2. In all cases, $\mu/\langle\Psi\rangle$ ranges from 0.2 to 0.4, indicating that the mean value consists primarily of the mean value of the pulses.

The pulse parameters $\tau_{\rm d}$ and λ can be estimated from the power spectral density and the conditionally averaged pulse shape of a time series. In the study by Garcia *et al.*,[26] it was found that a pulse shape with $\tau_{\rm d} = 20\,\mu$s and $\lambda = 1/10$ describes the power spectral density and conditional average of all data time series analyzed here well. These results are presented here to complete the parameter estimation.

TABLE II. Estimated model parameters from the GPI data time series.

Plasma state	γ	ϵ	μ	$\langle A\rangle$	$\langle\Psi\rangle$
lO	0.60	0.02	0.06	0.13	0.14
hO	1.71	0.01	0.08	0.06	0.19
qH	1.51	0.00	0.11	0.23	0.45
eH	3.30	0.00	0.24	0.18	0.84

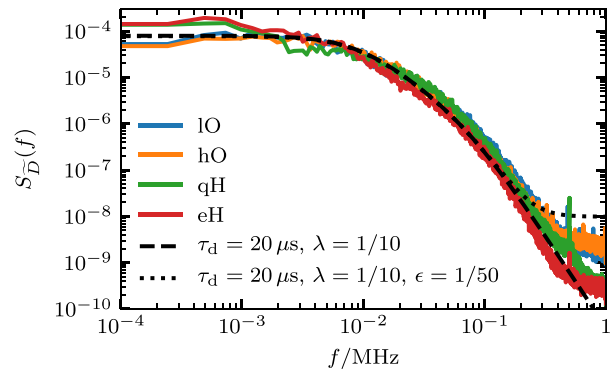

FIG. 3. Power spectral density of GPI measurement data. The black lines give the prediction from the stochastic model. The black dashed line does not include noise, while the black dotted line includes noise with noise parameter $\epsilon = 1/50$.[26]

In Fig. 3, the power spectral densities for the four different plasma states are presented together with the analytical prediction of the power spectrum of an FPP, both with (black dotted line) and without (black dashed line) additive noise.[42] The power spectra show a remarkable similarity and agree with the prediction from the stochastic model using $\tau_{\rm d} = 20\,\mu$s and $\lambda = 1/10$. The tail of the power spectra rises for the largest frequencies, but this is consistent with a noise level between 0 and 0.02. The universality of the power spectra from GPI time series from the SOL of Alcator C-Mod for different line-averaged densities and confinement regimes and at different radial positions in the SOL has been noted before.[25,26]

In order to verify the deconvolution method, we will employ it on a synthetically generated FPP with additive noise with parameters $\gamma = 3/2$, $\tau_{\rm d} = 20\,\mu$s, $\lambda = 1/10$, and $\epsilon = 1/100$ in addition to the GPI data. In the following, this realization will be denoted Ψ_K. In Fig. 4, the conditionally averaged waveform for the four different plasma states is presented together with the conditional average of Ψ_K. The conditional average of the synthetic signal conforms well to

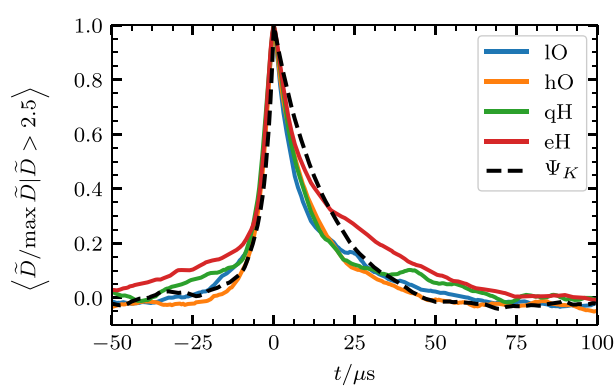

FIG. 4. Conditionally averaged waveform of GPI measurements and synthetic data for fluctuation amplitudes larger than 2.5 times the root mean square value.[26]

the general shape of the conditional average of the data time series. The somewhat longer duration time of the enhanced D-alpha H-mode case was discussed in the study by Garcia *et al.*[26] and is not taken to be significant for the purposes of the deconvolution. Indeed, as the deconvolution is robust to small deviations in the pulse shape, we will use $\tau_d = 20\ \mu s$ and $\lambda = 1/10$ as the pulse parameters for the deconvolution of all measurement data time series. Different pulse parameters have been tested, without significant deviations in the results presented in Sec. V.

IV. DECONVOLUTION ALGORITHM

The FPP can be written as a convolution between the pulse function and a train of delta-function pulses[42]

$$\Phi_K(t) = [\varphi * f_K]\left(\frac{t}{\tau_d}\right), \tag{7}$$

where

$$f_K(t) = \sum_{k=1}^{K(T)} A_k \delta\left(\frac{t - t_k}{\tau_d}\right). \tag{8}$$

The goal of this contribution is to obtain and investigate the properties of the pulse amplitudes $\{A_k\}_{k=1}^K$ and arrival times $\{t_k\}_{k=1}^K$ directly. In order to do this, we will take as a starting point the Richardson-Lucy deconvolution algorithm[45,46] with normally distributed noise[47–50] to estimate $f_K(t)$. This algorithm is iterative, with the $n+1$'th iteration given by

$$f_K^{(n+1)} = f_K^{(n)} \frac{(D - \mu) * \widehat{\varphi}}{f_K^{(n)} * \varphi * \widehat{\varphi}}, \tag{9}$$

where $\widehat{\varphi}(t) = \varphi(-t)$. Here and in the following, D denotes any of the GPI measurement data time series discussed above and the realization Ψ_K discussed below. The estimate of μ is presented in Table II. We note that Eq. (9) is independent of X_{rms}. The initial guess $f_K^{(0)}$ is unimportant and can be set as a positive constant or the measurement signal itself.

If D–μ and $f_K^{(0)}$ are positive definite, each iteration $f_K^{(n)}$ is as well. While D is positive definite and $f_K^{(1)}$ can be chosen positive definite, D–μ is not guaranteed to be positive definite. In practice, however, the noise level is small enough that using the absolute value of D–μ has no appreciable effect on the result of the deconvolution (the power contained in the negative part of D–μ is less than 1% of the total signal power). The algorithm converges to the least-squares solution.[49] The result of the iteration is a super-position of sharp Gaussian-like pulses, as the iteration gradually smoothens the signal. The arrival times are determined from the maxima of $f_K^{(n)}$. The amplitudes associated with each arrival are the integral of $f_K^{(n)}$ from the minima between the previous and current arrivals to the minima between the current and next arrivals. The reconstructed data time series, D_{rec}, is then computed from these arrival times and amplitudes according to Eq. (2)

The maxima of $f_K^{(n)}$ are determined as the zeros in the derivative of $f_K^{(n)}$, where the derivative is computed by fitting $f_K^{(n)}$ to a second-order polynomial in a prescribed window. The number of detected arrivals depends strongly on the window size, and we choose a window size such that the difference between the number of deconvolved events and the expected number of events is minimized. If we were to use the expected total number of events, $\langle K \rangle = \gamma T/\tau_d$, we would ignore the fact that events may arrive closer than a sampling time. For a discrete time grid superposed on a continuous, homogeneous Poisson process, the expected number of time grid points containing pulse arrivals is $\langle F \rangle = N[(1 - \exp(-\gamma \triangle_t/\tau_d)]$, where $N = T/\tau_d$ is the number of time grid points and $\triangle_t$ is the time step.[51] Since the deconvolution procedure only discovers the presence of events at a given grid point, $\langle F \rangle$ is the correct number of events to use. We choose the window size minimizing the difference between the number of deconvolved events and $\langle F \rangle$. In the case of the GPI time series, the window sizes are 28.5 μs (lO), 7.5 μs (hO), 6.5 μs (qH), and 5.5 μs (eH), giving 2990, 8012, 7271, and 15507 events, respectively. By comparison, conditional averaging of these time series is obtained on the order of one hundred events. For the synthetic time series, a window of 8.5 μs was used, giving 7485 events in comparison to 196 events from conditional averaging. Increasing the window size eliminates small and sharp peaks in $f_K^{(n)}$ and consolidates close peaks. This comprises the noise handling inherent in the method.

V. RESULT OF DECONVOLUTION

The result of the deconvolution algorithm is presented in Fig. 1, with the reconstructed time series plotted on top of the measurement data. In all cases, the reconstructed signal is very close to the original signal. The PDFs also correspond closely, as seen in Fig. 2. An excerpt of the low density Ohmic case with the reconstructed signal and pulse amplitudes is presented in Fig. 5. While there is some scatter around the measured signal, the reconstruction captures the main fluctuations in the GPI signal.

The pulse amplitude distribution is presented in Fig. 6 for all plasma parameters and confinement modes, as well as for the synthetically generated signal. These PDFs correspond closely to an exponential distribution over more than two decades in probability. Note that the excess probability for small amplitudes is also present in the synthetically

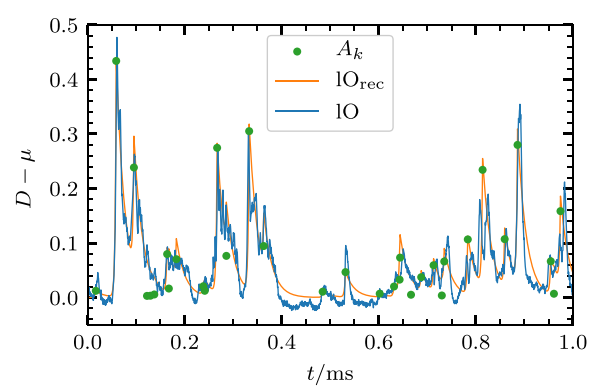

FIG. 5. Excerpt of measurement data (blue line) and reconstructed time series (orange line) for the low density Ohmic state. The green dots show the estimated pulse arrival times and amplitudes.

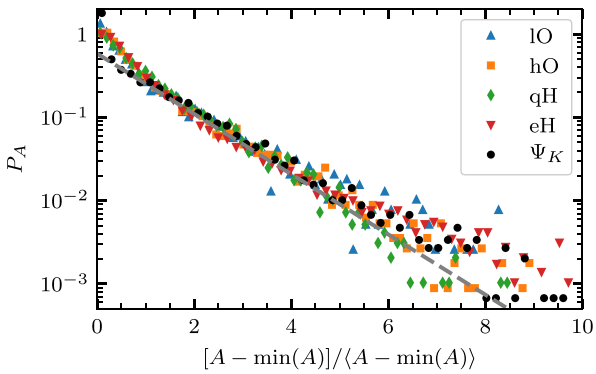

FIG. 6. PDF of pulse amplitudes estimated from the deconvolution algorithm for various plasma parameters and confinement states. The grey dashed line indicates the exponential decay.

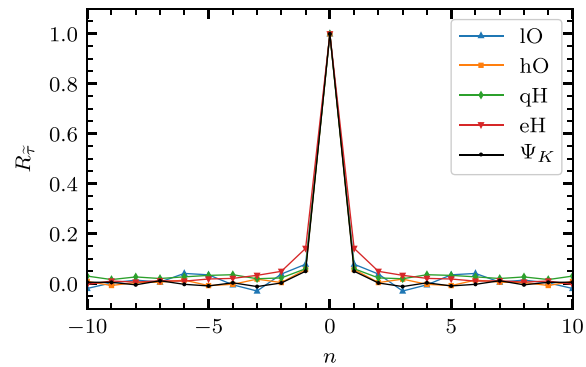

FIG. 8. Auto-correlation function of waiting times between pulses estimated from the deconvolution algorithm for various plasma parameters and confinement states.

generated signal. From these distributions, we find that $\langle A\rangle$ for the reconstructed time series is 0.14 (lO), 0.07 (hO), 0.24 (qH), and 0.19 (eH). Comparing these values with the ones given in Table II, we see that the deconvolution is fully consistent with estimation using the moments of the data time series.

In Fig. 7, the waiting time distribution is presented for all plasma parameters and confinement modes, as well as for the synthetically generated signal. The gray dashed line gives an exponential distribution. All distributions follow an exponential function for long waiting times, and the deviation from the exponential distribution for short waiting times is shared by the synthetically generated signal. The average waiting time for these distributions (in μs) is 33 (lO), 12 (hO), 14 (qH), and 6.4 (eH). For the data time series, τ_w can be estimated as $\tau_w = \tau_d/\gamma$. Using γ from Table II and $\tau_d = 20$ μs, we find that τ_w for the data time series is 33 (lO), 12 (hO), 13 (qH), and 6.1 (eH). Again, these results are fully consistent.

The auto-correlation function of the consecutive waiting times is presented in Fig. 8, where $R_{\tilde{\tau}}[n] = R_{\tilde{\tau}}[k, k+n] = \langle \tilde{\tau}_k\, \tilde{\tau}_{k+n}\rangle$, and τ is normalized according to Eq. (1) in order to properly normalize the auto-correlation function. As this is a delta function, consecutive waiting times are uncorrelated and therefore independently distributed. In Fig. 9, the number of arrivals K as a function of elapsed time t is presented for all datasets. This follows a linear function, showing that the mean value of K can be written as $\langle K(t)\rangle = t/\tau_w$, consistent with a homogeneous Poisson process.

The assumptions of the FPP model are that the number of arrivals follows a homogeneous Poisson process with a constant average waiting time τ_w. Using the fact that the waiting times are independent and that for $\tau > \langle\tau\rangle$, they are exponentially distributed, it follows that the process $f_K(t)$ has independent increments and that the number of arrivals $K(t)$ is Poisson distributed for all $t \in [0, T]$. The linearity of $K(t)$ shows that τ_w is constant in time. Thus, the process $K(t)$ is a Poisson process with a constant rate of arrivals.

Denoting the reconstructed signals as D_{rec}, the *residual* $D_{res} = (D - \mu) - D_{rec}$ contains both the error in the reconstruction and the parts of the time series not describable by the FPP. In Fig. 10, the PDFs of the residuals are presented, normalized by the rms-value of the original signal such that Fig. 10 can be directly compared with Fig. 2. These distributions are all sharply peaked and nearly symmetric around the zero-value. The low-density ohmic case has a broader distribution than the other cases, reflecting more pronounced over- and under-estimation of large fluctuations. This difference is likely due to the higher intermittency of the low-density ohmic case compared to the other cases. To show this, a new synthetic time series with $\gamma = 2/3$ and all other parameters the same as before has been generated and reconstructed, and the PDF of its residual is plotted in Fig. 10. It is clear that higher intermittency leads to larger residual values. For strongly intermittent signals, individual deviations from

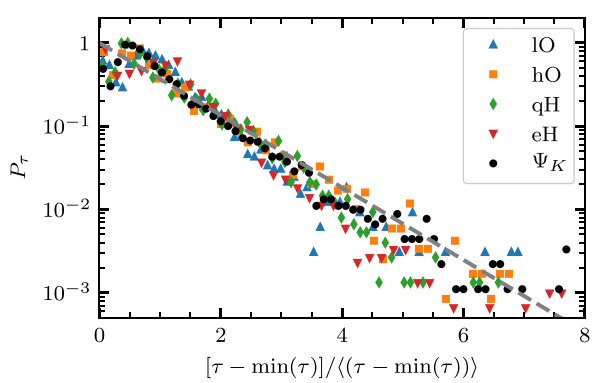

FIG. 7. PDF of waiting times between pulses estimated from the deconvolution algorithm for various plasma parameters and confinement states. The grey dashed line gives an exponential distribution.

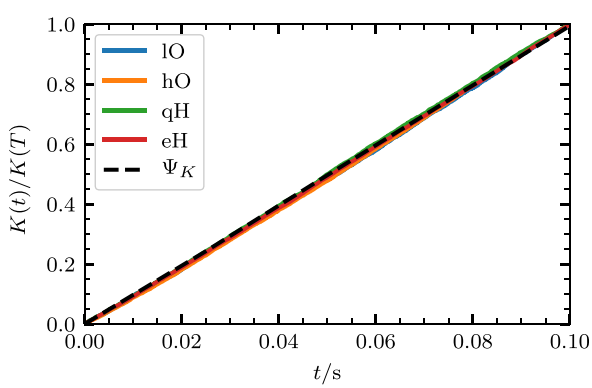

FIG. 9. Number of pulse arrivals as a function of time estimated from the deconvolution algorithm for various plasma parameters and confinement states.

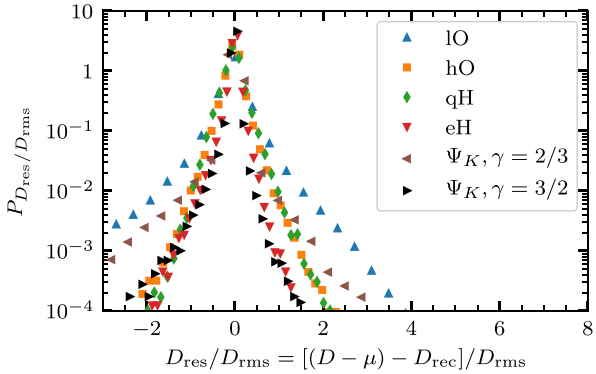

FIG. 10. Probability density functions of the residual of the deconvolution algorithm for various plasma parameters and confinement states.

the average exponential shape of the bursts are more pronounced, and so, estimation of single pulses is more variable. Note that none of the distributions are normally distributed, and all seem to follow the same type of distribution as the residual from the synthetic signals. In the study by Theodorsen and Garcia,[51] it will be argued that due to the exponential amplitude distributions and the Gamma distribution of the FPP, normally distributed residuals are not to be expected.

In Fig. 11, the PSD of the residual time series is presented. For low frequencies, below about 10 kHz, the power density is very moderate, below 1% of the power contained in comparable frequencies for the data time series, Fig. 3. On the other hand, the power content at high frequencies, above about 10^2 kHz, is comparable to that of the data time series as a whole. This may be due to high-frequency noise filtered out by the deconvolution algorithm. The residual of the low-density ohmic case contains the most power, consistent with the broader PDF in Fig. 10. We again conclude from comparing the residuals of the two synthetically generated signals that a lower γ leads to larger differences between the original and reconstructed signals, which is evident from the higher power contained in the more intermittent signal.

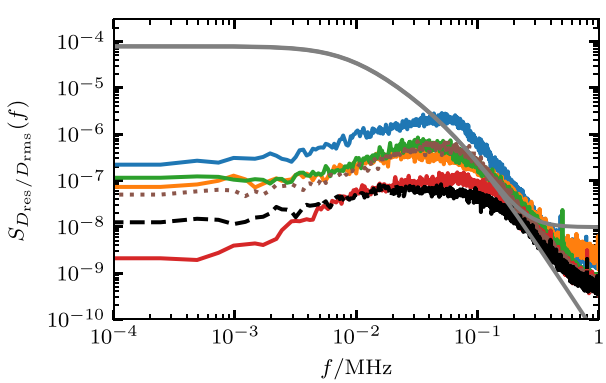

FIG. 11. Power spectral densities of the residual of the deconvolution algorithm for various plasma parameters and confinement states. The color coding is the same as in Fig. 3. The residual of the synthetic signals Ψ_K with $\gamma = 3/2$ and $\gamma = 2/3$ is given by the black dashed line and the brown dotted line, respectively. The grey full line gives the prediction of the FPP with pulse parameters $\tau_d = 20$ μs and $\lambda = 1/10$. The monotonically decaying part is noiseless and the part which flattens for high frequencies includes additive noise with $\epsilon = 2 \times 10^{-2}$, as in Fig. 3.

VI. DISCUSSION

In the study by Garcia *et al.*,[26] the peak amplitudes and the corresponding arrival times of conditional events from a conditional averaging procedure were recorded and used to provide an estimate of the shape of the PDFs of A and τ for the dataset analyzed in this contribution. Figures 6 and 7 in this contribution are compared with Figs. 9 and 10 in the study by Garcia *et al.*[26] Deconvolution provides two advantages over peak finding from conditional averaging: first, the number of found events is one to two orders of magnitude higher, giving clearer distributions over more decades in probability. Second, the moments of the deconvolved amplitudes and waiting times can be used directly for comparison with the moments of the original time series. This is not in general possible for the conditionally averaged events. However, it is also noteworthy that conditional averaging gives the same statistical properties for SOL fluctuations in Alcator C-Mod, KSTAR, and TCV.[22–24,26]

We reiterate that the deviation of the estimated P_A in Fig. 6 and P_τ in Fig. 7 from a pure exponential distribution is shared by a realization of a FPP. Thus, the results presented here fully support the conclusion that plasma fluctuations in the SOL of ACM can be described as an FPP with exponentially distributed amplitudes. Also note that while we can infer the FPP model parameters from the analysis presented in this contribution, these cannot be used to directly infer plasma parameters as GPI is a highly nonlinear function of the electron density and temperature.

In both Figs. 10 and 11, the synthetically generated signal with $\gamma = 3/2$ should be compared with the "hO"- and "qH"-cases, while the synthetically generated signal with $\gamma = 2/3$ should be compared with the "lO"-case. In both cases, the residuals of the measurement data time series contain higher probability of large values and more power than the residuals of the synthetically generated signals. This may be due to errors in the estimation of the model parameters, noise which does not conform to the prescribed noise or variability in the pulse shape not described by the model.

There are two caveats to the deconvolution method. First, as it can only detect the presence or absence of events (and the combined event amplitude) within a time step, the method becomes less effective for a higher degree of pulse overlap. As the pulse overlap increases, more events arrive within a single time step and fewer of the individual, original arrivals can be detected. The method is therefore of most use in the mid- to far-SOL where the intermittency is significant as opposed to near the separatrix where the fluctuations are close to normally distributed. Second, only events with positive amplitudes can be detected, which excludes investigation of, for instance, electric potential fluctuations in the far-SOL and blob-hole formation near the separatrix (which was already problematic due to the near-Gaussian signals).

VII. CONCLUSIONS

The FPP with exponentially shaped pulses and exponentially distributed pulse amplitudes has previously successfully predicted all statistical properties of SOL fluctuations as recoded by single-point measurements. This comprises

the amplitude PDF,[21–26,52–54] the auto-correlation function, the frequency power spectral density,[23–26] level crossing rates, and excess time statistics[24,25] as well as conditional pulse shape, pulse amplitude distributions, and inter-pulse waiting times from conditional averaging.[22–26,52–54]

In this contribution, a deconvolution algorithm is used in order to directly and unambiguously recover pulse amplitudes and arrival times, verifying the underlying assumptions of the stochastic model. This algorithm is applied to GPI data time series that recorded emission fluctuations in the SOL of the Alcator C-Mod device for various plasma parameters and confinement modes. The statistical properties of far-SOL fluctuation pulse arrival times and amplitudes have been shown to be the same in all cases. Both the pulse amplitudes and the waiting times are exponentially distributed. Moreover, the waiting times are uncorrelated and the number of pulse arrivals increases linearly with the time series duration. This demonstrates that the statistics of far-SOL fluctuations are the same for ohmic and H-mode plasmas in the Alcator C-Mod device and in particular that the pulses arrive according to a homogeneous Poisson process and have exponentially distributed amplitudes, confirming all the assumptions underlying the stochastic model. This provides strong evidence in the support of universal applicability of the stochastic model, providing a valuable tool for describing intermittent fluctuations and associated plasma–wall interactions in the boundary region of magnetically confined plasmas. The properties of the deconvolution algorithm will be elucidated in a separate contribution.[51]

ACKNOWLEDGMENTS

This work was supported by financial subvention from the Research Council of Norway under Grant No. 240510/F20 and the U.S. Department of Energy, Office of Science, Office of Fusion Energy Sciences, using User Facility Alcator C-Mod, under Award No. DE-FC02-99ER54512-CMOD. A.T., O.E.G., and R.K. acknowledge the generous hospitality of the MIT Plasma Science and Fusion Center where parts of this work were conducted.

[1]D. A. D'Ippolito, J. R. Myra, S. I. Krasheninnikov, G. Q. Yu, and A. Y. Pigarov, Contrib. Plasma Phys. **44**, 205 (2004).
[2]S. J. Zweben, J. A. Boedo, O. Grulke, C. Hidalgo, B. LaBombard, R. J. Maqueda, P. Scarin, and J. L. Terry, Plasma Phys. Controlled Fusion **49**, S1 (2007).
[3]S. I. Krasheninnikov, D. A. D'Ippolito, and J. R. Myra, J. Plasma Phys. **74**, 679 (2008).
[4]O. E. Garcia, Plasma Fusion Res. **4**, 019 (2009).
[5]D. A. D'Ippolito, J. R. Myra, and S. J. Zweben, Phys. Plasmas **18**, 060501 (2011).
[6]B. LaBombard, R. L. Boivin, M. Greenwald, J. Hughes, B. Lipschultz, D. Mossessian, C. S. Pitcher, J. L. Terry, and S. J. Zweben, and the Alcator Group, Phys. Plasmas **8**, 2107 (2001).
[7]R. A. Pitts, J. P. Coad, D. P. Coster, G. Federici, W. Fundamenski, J. Horacek, K. Krieger, A. Kukushkin, J. Likonen, G. F. Matthews, M. Rubel, and J. D. Strachan, and JET-EFDA Contributors. Plasma Phys. Controlled Fusion **47**, B303 (2005).
[8]B. Lipschultz, X. Bonnin, G. Counsell, A. Kallenbach, A. Kukushkin, K. Krieger, A. Leonard, A. Loarte, R. Neu, R. Pitts, T. Rognlien, J. Roth, C. Skinner, J. Terry, E. Tsitrone, D. Whyte, S. Zweben, N. Asakura, D. Coster, R. Doerner, R. Dux, G. Federici, M. Fenstermacher, W. Fundamenski, P. Ghendrih, A. Herrmann, J. Hu, S. Krasheninnikov, G. Kirnev, A. Kreter, V. Kurnaev, B. LaBombard, S. Lisgo, T. Nakano, N. Ohno, H. Pacher, J. Paley, Y. Pan, G. Pautasso, V. Philipps, V. Rohde, D. Rudakov, P. Stangeby, S. Takamura, T. Tanabe, Y. Yang, and S. Zhu, Nucl. Fusion **47**, 1189 (2007).
[9]D. A. D'Ippolito and J. R. Myra, Phys. Plasmas **15**, 082316 (2008).
[10]Y. Marandet, N. Nace, M. Valentinuzzi, P. Tamain, H. Bufferand, G. Ciraolo, P. Genesio, and N. Mellet, Plasma Phys. Controlled Fusion **58**, 114001 (2016).
[11]B. LaBombard, J. Hughes, D. Mossessian, M. Greenwald, B. Lipschultz, and J. Terry, and the Alcator C-Mod Team, Nucl. Fusion **45**, 1658 (2005).
[12]G. Y. Antar, G. Counsell, and J. W. Ahn, Phys. Plasmas **12**, 082503 (2005).
[13]D. A. D'Ippolito and J. R. Myra, Phys. Plasmas **13**, 062503 (2006).
[14]O. E. Garcia, R. A. Pitts, J. Horacek, J. Madsen, V. Naulin, A. H. Nielsen, and J. J. Rasmussen, Plasma Phys. Controlled Fusion **49**, B47 (2007).
[15]P. N. Guzdar, R. G. Kleva, P. K. Kaw, R. Singh, B. LaBombard, and M. Greenwald, Phys. Plasmas **14**, 020701 (2007).
[16]O. E. Garcia, Phys. Rev. Lett. **108**, 265001 (2012).
[17]O. E. Garcia, R. Kube, A. Theodorsen, and H. L. Pécseli, Phys. Plasmas **23**, 052308 (2016).
[18]F. Militello and J. T. Omotani, Nucl. Fusion **56**, 104004 (2016).
[19]F. Militello and J. T. Omotani, Plasma Phys. Controlled Fusion **58**, 125004 (2016).
[20]A. Theodorsen and O. E. Garcia, Plasma Phys. Controlled Fusion **60**, 034006 (2018).
[21]J. P. Graves, J. Horacek, R. A. Pitts, and K. I. Hopcraft, Plasma Phys. Controlled Fusion **47**, L1 (2005).
[22]R. Kube, A. Theodorsen, O. E. Garcia, B. LaBombard, and J. L. Terry, Plasma Phys. Controlled Fusion **58**, 054001 (2016).
[23]A. Theodorsen, O. E. Garcia, J. Horacek, R. Kube, and R. A. Pitts, Plasma Phys. Controlled Fusion **58**, 044006 (2016).
[24]O. E. Garcia, R. Kube, A. Theodorsen, J.-G. Bak, S.-H. Hong, H.-S. Kim, the KSTAR Project Team, and R. A. Pitts, Nucl. Mater. Energy **12**, 36 (2017).
[25]A. Theodorsen, O. E. Garcia, R. Kube, B. LaBombard, and J. L. Terry, Nucl. Fusion **57**, 114004 (2017).
[26]O. E. Garcia, R. Kube, A. Theodorsen, B. LaBombard, and J. L. Terry, Phys. Plasmas **25**, 056103 (2018).
[27]R. Kube, O. E. Garcia, A. Theodorsen, D. Brunner, A. Q. Kuang, B. LaBombard, and J. L. Terry, Plasma Phys. Controlled Fusion **60**, 065002 (2018).
[28]N. R. Walkden, A. Wynn, F. Militello, B. Lipschultz, G. Matthews, C. Guillemaut, J. Harrison, and D. Moulton, Plasma Phys. Controlled Fusion **59**, 085009 (2017).
[29]D. L. Rudakov, J. A. Boedo, R. A. Moyer, S. Krasheninnikov, A. W. Leonard, M. A. Mahdavi, G. R. McKee, G. D. Porter, P. C. Stangeby, J. G. Watkins, W. P. West, D. G. Whyte, and G. Antar, Plasma Phys. Controlled Fusion **44**, 717 (2002).
[30]G. Y. Antar, M. Tsalas, E. Wolfrum, and V. Rohde, Plasma Phys. Controlled Fusion **50**, 095012 (2008).
[31]C. Ionita, V. Naulin, F. Mehlmann, J. Rasmussen, H. Müller, R. Schrittwieser, V. Rohde, A. Nielsen, C. Maszl, P. Balan, and A. Herrmann, Nucl. Fusion **53**, 043021 (2013).
[32]S. Zweben, W. Davis, S. Kaye, J. Myra, R. Bell, B. LeBlanc, R. Maqueda, T. Munsat, S. Sabbagh, Y. Sechrest, and D. Stotler, Nucl. Fusion **55**, 093035 (2015).
[33]S. J. Zweben, J. R. Myra, W. M. Davis, D. A. D'Ippolito, T. K. Gray, S. M. Kaye, B. P. LeBlanc, R. J. Maqueda, D. A. Russell, and D. P. Stotler, Plasma Phys. Controlled Fusion **58**, 044007 (2016).
[34]I. Cziegler, J. L. Terry, J. W. Hughes, and B. LaBombard, Phys. Plasmas **17**, 056120 (2010).
[35]M. Greenwald, J. L. Terry, S. M. Wolfe, S. Ejima, M. G. Bell, S. M. Kaye, and G. H. Neilson, Nucl. Fusion **28**, 2199 (1988).
[36]B. LaBombard, T. Golfinopoulos, J. L. Terry, D. Brunner, E. Davis, M. Greenwald, and J. W. Hughes, Phys. Plasmas **21**, 056108 (2014).
[37]M. Greenwald, R. Boivin, F. Bombarda, P. Bonoli, C. Fiore, D. Garnier, J. Goetz, S. Golovato, M. Graf, R. Granetz, S. Horne, A. Hubbard, I. Hutchinson, J. Irby, B. LaBombard, B. Lipschultz, E. Marmar, M. May, G. McCracken, P. O'Shea, J. Rice, J. Schachter, J. Snipes, P. Stek, Y. Takase, J. Terry, Y. Wang, R. Watterson, B. Welch, and S. Wolfe, Nucl. Fusion **37**, 793 (1997).
[38]M. Greenwald, A. Bader, S. G. Baek, M. Bakhtiari, H. Barnard, W. Beck, W. Bergerson, I. Bespamyatnov, P. Bonoli, D. Brower, D. Brunner, W. Burke, J. Candy, M. Churchill, I. Cziegler, A. Diallo, A. Dominguez, B. Duval, E. Edlund, P. Ennever, D. Ernst, I. Faust, C. Fiore, T. Fredian, O. E. Garcia, C. Gao, J. Goetz, T. Golfinopoulos, R. Granetz, O. Grulke, Z.

Hartwig, S. Horne, N. Howard, A. Hubbard, J. Hughes, I. Hutchinson, J. Irby, V. Izzo, C. Kessel, B. LaBombard, C. Lau, C. Li, Y. Lin, B. Lipschultz, A. Loarte, E. Marmar, A. Mazurenko, G. McCracken, R. McDermott, O. Meneghini, D. Mikkelsen, D. Mossessian, R. Mumgaard, J. R. Myra, E. Nelson-Melby, R. Ochoukov, G. Olynyk, R. Parker, S. Pitcher, Y. Podpaly, M. Porkolab, M. Reinke, J. Rice, W. Rowan, A. Schmidt, S. Scott, S. Shiraiwa, J. Sierchio, N. Smick, J. A. Snipes, P. Snyder, B. Sorbom, J. Stillerman, C. Sung, Y. Takase, V. Tang, J. L. Terry, D. Terry, C. Theiler, A. Tronchin-James, N. Tsujii, R. Vieira, J. Walk, G. Wallace, A. White, D. Whyte, J. Wilson, S. Wolfe, G. Wright, J. Wright, S. Wukitch, and S. J. Zweben, Phys. Plasmas **21**, 110501 (2014).

[39]K. H. Burrell, T. H. Osborne, P. B. Snyder, W. P. West, M. E. Fenstermacher, R. J. Groebner, P. Gohil, A. W. Leonard, and W. M. Solomon, Phys. Rev. Lett. **102**, 155003 (2009).

[40]R. Kube and O. E. Garcia, Phys. Plasmas **22**, 012502 (2015).

[41]A. Theodorsen and O. E. Garcia, Phys. Plasmas **23**, 040702 (2016).

[42]A. Theodorsen, O. E. Garcia, and M. Rypdal, Phys. Scr. **92**, 054002 (2017).

[43]O. E. Garcia and A. Theodorsen, Phys. Plasmas **24**, 032309 (2017).

[44]A. Theodorsen and O. E. Garcia, Phys. Rev. E **97**, 012110 (2018).

[45]W. H. Richardson, J. Opt. Soc. Am. **62**, 55 (1972).

[46]L. B. Lucy, Astron. J. **79**, 745 (1974).

[47]M. E. Daube-Witherspoon and G. Muehllehner, IEEE Trans. Med. Imaging **5**, 61 (1986).

[48]M. Pruksch and F. Fleischmann, in *Astronomical Data Analysis Software Systems - VII*, Astronomical Society of the Pacific Conference Series edited by R. Albrecht, R. N. Hook, and H. A. Bushouse (Astronomical Society of the Pacific, 1998), pp. 496–499.

[49]F. Dell'Acqua, G. Rizzo, P. Scifo, R. A. Clarke, G. Scotti, and F. Fazio, IEEE Trans. Biomed. Eng. **54**, 462 (2007).

[50]Y.-W. Tai, P. Tan, and M. S. Brown, IEEE Trans. Pattern Anal. Mach. Intell. **33**, 1603 (2011).

[51]A. Theodorsen and O. E. Garcia, "A deconvolution method for reconstruction of data time series from intermittent systems," e-print arXiv:1811.11033 (unpublished).

[52]O. E. Garcia, I. Cziegler, R. Kube, B. LaBombard, and J. L. Terry, J. Nucl. Mater. **438**, S180 (2013).

[53]O. E. Garcia, S. M. Fritzner, R. Kube, I. Cziegler, B. LaBombard, and J. L. Terry, Phys. Plasmas **20**, 055901 (2013).

[54]O. E. Garcia, J. Horacek, and R. A. Pitts, Nucl. Fusion **55**, 062002 (2015).